Article

Synaptobrevin Transmembrane Domain Dimerization Studied by Multiscale Molecular Dynamics Simulations

Jing Han,[1] Kristyna Pluhackova,[1] Tsjerk A. Wassenaar,[1] and Rainer A. Böckmann[1,*]
[1]Computational Biology, Department of Biology, Friedrich-Alexander Universität Erlangen-Nürnberg, Erlangen, Germany

ABSTRACT Synaptic vesicle fusion requires assembly of the SNARE complex composed of SNAP-25, syntaxin-1, and synaptobrevin-2 (sybII) proteins. The SNARE proteins found in vesicle membranes have previously been shown to dimerize via transmembrane (TM) domain interactions. While syntaxin homodimerization is supposed to promote the transition from hemifusion to complete fusion, the role of synaptobrevin's TM domain association in the fusion process remains poorly understood. Here, we combined coarse-grained and atomistic simulations to model the homodimerization of the sybII transmembrane domain and of selected TM mutants. The wild-type helix is shown to form a stable, right-handed dimer with the most populated helix-helix interface, including key residues predicted in a previous mutagenesis study. In addition, two alternative binding interfaces were discovered, which are essential to explain the experimentally observed higher-order oligomerization of sybII. In contrast, only one dimerization interface was found for a fusion-inactive poly-Leu mutant. Moreover, the association kinetics found for this mutant is lower as compared to the wild-type. These differences in dimerization between the wild-type and the poly-Leu mutant are suggested to be responsible for the reported differences in fusogenic activity between these peptides. This study provides molecular insight into the role of TM sequence specificity for peptide aggregation in membranes.

INTRODUCTION

Neurotransmitter release requires a rapid and precise fusion of synaptic vesicles with the presynaptic plasma membrane. The fusion is mediated by a set of conserved proteins collectively known as the soluble *n*-ethylmaleimide-sensitive-factor attachment receptor (SNARE) complex (1–3). The protein complex that is formed upon fusion consists of the membrane-peripheral protein SNAP-25 and the two integral membrane proteins synaptobrevin-2 (sybII) and syntaxin. The latter two are anchored to their respective host membranes by single-pass transmembrane domains (TMDs) while SNAP-25 is attached to the membrane by a lipidic anchor. SybII is localized on the vesicle membrane while syntaxin and SNAP-25 are located on the plasma membrane. The assembly of SNARE proteins to a *trans*-complex bridges the two opposing membranes and drives membrane fusion. A crystal structure of the SNARE complex shows a parallel four-helix bundle assembled from the cytoplasmic regions of the SNARE proteins (4). The continuous zippering of this complex beyond the core complex extending all the way into the transmembrane region leads to a highly stable *cis* complex, with all SNARE proteins located in the same fused membrane (5). This directional transition is believed to act as a force-generating machine and to be responsible for the final membrane merging (6,7). However, the mechanism by which SNARE induces membrane fusion remains elusive.

Apart from the role of the soluble domains of SNARE proteins in mediating the formation of a SNARE complex, various studies have shown that the TMDs of SNAREs play an essential role in membrane fusion and complex oligomerization (8–13). Incorporation of synthetic peptides into liposomes mimicking these transmembrane domains of SNARE proteins was shown to induce fusion in vitro, suggesting an important role of specific TMD-TMD interactions in mediating the fusion reaction (14). Additionally, homo- and heterodimerization of SNARE proteins (both syntaxin and sybII) have been reported to be mediated by interactions between TMDs, in a sequence-specific fashion (15–18). Additionally, signals for homotrimers and -tetramers were reported for fusion constructs consisting of nuclease A and the sybII TM segment (17). For sybII, six residues (L99, I102, C103, L107, I110, and I111) have been predicted to reside at the dimer interface and to be responsible for the formation of stable dimers, as evidenced from previous mutagenesis and computational studies (17,19). Only weak sybII homodimerization was seen using the method TOXCAT (20), causing a questioning of the biological relevance of TMD association in membrane fusion. This system was later reinvestigated yielding a substantial propensity of sybII for dimer formation (21). Additionally, dimerization of sybII was revealed in a bimolecular fluorescence complementation approach, albeit the dimerization appeared not to contribute to fusion activity in vivo as fusion was not affected by a mutation that abolished dimerization (G100V and G100Y (11)). In turn, Hofmann et al. (22) suggested that the TMD-TMD interaction promotes the

Submitted April 22, 2015, and accepted for publication June 25, 2015.
*Correspondence: rainer.boeckmann@fau.de
Editor: Scott Feller.

0006-3495/15/08/0760/12
http://dx.doi.org/10.1016/j.bpj.2015.06.049

hemifusion-to-fusion transition. Also, it was shown that the stoichiometry of yeast SNARE TMD oligomers is at least three (12). Although these studies suggest that the TMD of SNARE plays a significant role in membrane fusion (23), the mechanism of self-association of TMDs, and the underlying structural basis as well as functional relevance of oligomerization, are not well understood.

Considering the difficulty in obtaining high-resolution structural information of membrane proteins, different computational approaches have been proven as insightful alternatives in studying the structure and dynamics of TMD associations (19,24–26). For example, multiple binding modes have been discovered for the fibroblast growth factor receptor 3 TMD association by molecular-dynamics (MD) simulations, and these were consistent with the experimental model (25). For the TMD of sybII, a right-handed dimer with a crossing angle of −38° was modeled, with the interaction interface being in agreement with alanine mutagenesis data (19). Here, we applied a multiscale approach combining coarse-grained MD and subsequent atomistic simulations to investigate TMD-TMD dimerization of the sybII wild-type and mutants thereof to characterize the sequence-dependency of TMD association and for structural analysis of obtained dimer conformations. The predicted sybII dimer structure from this unbiased association study is in good agreement with previous computational and mutagenesis data. Additionally, two alternative binding modes are described that are suggested to be involved in SNARE oligomerization. Altering TMD residues led to an increased (poly-Val mutant) or a decreased (poly-Leu) dimerization propensity, while an interfacial tryptophan mutant (W89A-W90A) showed dimerization characteristics similar to the wild-type. These results contribute to an improved understanding of the role of TMD-TMD interactions in SNARE-mediated membrane fusion.

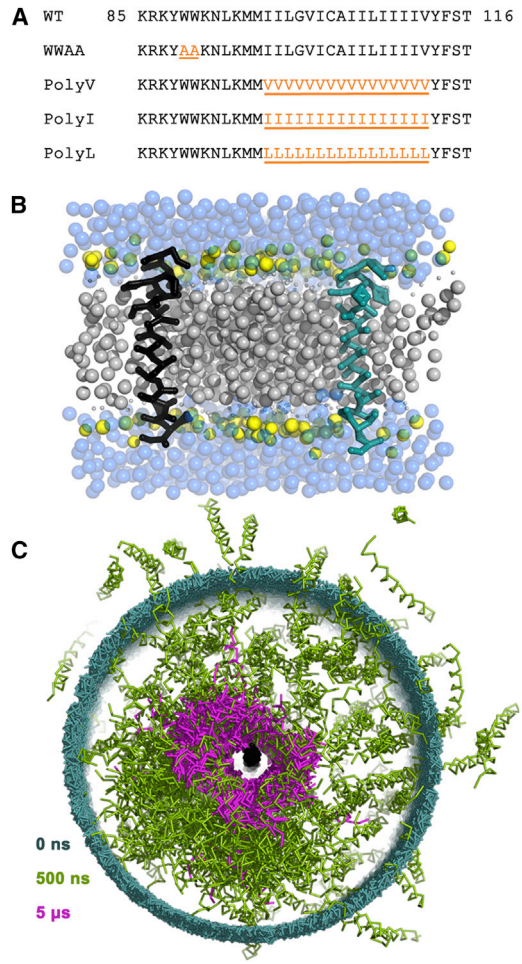

FIGURE 1 (*A*) Sequences of sybII wild-type and mutant helices used in the simulations. The mutated positions are underlined and colored (*orange*) in the sequences. (*B*) Starting configuration of a CG-WT simulation with two helices in stick representation (*black* and *cyan*) embedded in a POPC bilayer (headgroup and tail shown in *yellow* and *silver spheres*, respectively; water is represented by *blue spheres*). (*C*) Top view of helix-helix configurations after fit on one helix (*black*, in the center) for starting structures of CG simulations (*blue*); after 500 ns of simulation (*green*); and after 5 μs (*magenta*). To see this figure in color, go online.

MATERIALS AND METHODS

Ensembles of coarse-grained (CG) simulations were employed to study unbiased sybII TMD association. Selected obtained dimer conformations were subsequently validated in atomistic MD simulations. All simulations started from the wild-type (wt) and mutated sequences of the TMD of sybII (residues 85–116) in a lipid bilayer. The mutants included a tryptophan double-mutant previously shown to affect priming of synaptic vesicles (W89A, W90A) (27), as well as mutants addressing the sequence-specificity of the part of sybII located within the hydrophobic core of the membrane (residues 97–112). These core residues were replaced by either valine (PolyV mutant), isoleucine (PolyI mutant), or leucine (PolyL mutant) (Fig. 1 *A*).

Coarse-grained simulations

The coarse-grained methodology of the MARTINI force field (28) was employed for all association studies of the wt sybII. The association propensity of sybII and of the mutants was analyzed based on ensembles of CG association simulations generated using our recently developed docking assay for transmembrane (DAFT) components protocol for association studies of transmembrane proteins (29) or for adsorption studies on membrane interfaces (30). In brief, this method assists in the setup and analysis of a large number of association simulations starting from unbiased noninteracting initial states (see below). All simulations were set up starting from either the wt sybII TMD or from one of the four studied mutants (see Fig. 1 *A*). For each sequence, dimerization profiles were built from 500 simulations of 5 μs in a POPC bilayer. All simulations were performed using the software GROMACS, Ver. 4.5.2 (31).

Starting from the TMD sequences, DAFT first built idealized atomistic helices, using the software PYMOL (32), which were subsequently coarse-grained using the software MARTINIZE (28). The resulting coarse-grained helices were placed on the corresponding two-component (checkerboard) layout, at a center-of-mass (COM) COM-COM distance of ~4.5 nm and with random in-plane rotations to ensure that the starting ensemble has no bias toward a particular bound state. If one chain is taken as reference and used to align the ensemble, this yields a distribution of starting positions as shown in blue in Fig. 1 *C*. For each configuration

with two parallel TMD helices, a surrounding POPC bilayer and solvent (standard MARTINI water model, see Fig. 1 *B*) were built using the software INSANE (33,34), yielding systems with ~110 lipids, 1280 solvent molecules, and a total of 2900 particles.

The resulting systems were processed with the software MARTINATE (35), which first performed a 500-steps steepest-descent energy minimization, followed by a short (10-ps) simulation with position restraints on the protein beads together with a short time step of 2 fs to relax the membrane environment. Production MD simulations of 5 μs in length were performed in the NpT ensemble. The temperature was controlled by weak coupling to an external heat bath of 310 K, using the Bussi velocity rescale thermostat (36) with a coupling time of 1.0 ps, and the pressure was coupled semiisotropically to an external reference pressure of 1.0 bar using the Berendsen barostat (37), with a coupling time of 3.0 ps and a compressibility of 3.0×10^{-4} bar^{-1}. Electrostatic interactions were switched to zero between 0 and 1.2 nm, while Lennard-Jones interactions were switched to zero between 0.9 and 1.2 nm. Neighbor-lists for calculation of short-range interactions were updated every 10 steps. Water was modeled using the standard MARTINI water model, with a relative dielectric permittivity of 15. An integration time step of 20 fs was used and coordinates were written out every 500 ps. A 5-μs CG simulation (~2900 CG atoms) took ~17 h on eight cores (Xeon 2660v2 chip; Intel, Mountain View, CA).

Atomistic MD simulations

Representative structures obtained from the CG association simulations were converted to atomistic resolution using the BACKWARD algorithm (38). The resolution switching covered the whole system, i.e., proteins, POPC molecules, and water molecules, adopting the periodic box setup from the respective CG simulation. To avoid any bias due to a specific force field, the complex stability was investigated and compared for two different atomistic force fields, namely CHARMM36 (39) and a combination of AMBER99sb-ILDN (40) for the proteins and SLIPIDS (41,42) for the lipid molecules. Before simulation, the resulting atomistic systems were energy-minimized and equilibrated for 2 ns with restraints on the protein backbone atoms. The pressure was coupled semiisotropically to a pressure bath at 1 bar using the Parrinello-Rahman barostat (43). The temperature was maintained at 310 K using the Nosé-Hoover thermostat (44,45). The time constant for the temperature and pressure coupling was chosen as 1 ps in the CHARMM36 force field, while 0.5 and 10.0 ps were applied for temperature and pressure coupling, respectively, in the AMBER99sb-ILDN force field. Bond lengths were constrained using the LINCS algorithm (46) differently for CHARMM36 (H-bonds only) and AMBER/SLIPIDS (all bonds). Long-range Coulomb interactions were treated using particle-mesh Ewald (47) summation beyond a cutoff of 1.2 nm. The van der Waals interaction was switched to zero between 0.8 and 1.2 nm. The time step used for integration of the Newton equations of motion was set to 2 fs and the neighbor-list was updated every 10 steps. The final production MD simulations were conducted for 200 ns using the software GROMACS, Ver. 4.5.2 (31). The trajectories were analyzed using GROMACS tools and in-house codes. The atomistic simulations (>31,000 atoms) were run on 96 cores (Xeon 5650 chip; Intel); a 200-ns simulation took ~84 h.

Analysis

Potential-of-mean-force calculation

The potential-of-mean-force (PMF) calculation was used to energetically characterize different states. The PMF may be computed by integrating the mean force along an arbitrary path connecting two states, e.g., by using umbrella sampling (48). Alternatively, it can be obtained from the population density between the two states at equilibrium according to

$$\omega(\zeta) - \omega(\zeta^*) = -k_B T \ln \frac{P(\zeta)}{P(\zeta^*)},$$

where $\omega(\zeta)$ is the PMF in state ζ; $P(\zeta)/P(\zeta^*)$ is the density of states, ζ /ζ^*; k_B is the Boltzmann constant; and T is the temperature. The calculation of PMF profiles from unbiased simulations as generated with DAFT has been reported recently (49). Obtained PMF profiles for a poly-Ala peptide were consistent with results from the conventional umbrella sampling method, however, for the studied peptide even at reduced computational costs. Here, the one-dimensional PMF for TMD dimerization was calculated using the interhelical distance between the centers of mass (COM) of the two helices as a reaction coordinate. The population densities were binned with a width of 0.05 nm. Convergence issues were assessed by analyzing the PMF for time windows of 100-ns length each (corresponding to 200 structures) at different points in time between 500 ns and 5 μs.

Packing-density distribution

A packing-density distribution was calculated to describe the packing properties of the two sybII TMD helices in the CG simulations for the wild-type and the mutants. To that end, all trajectories were fitted on the first sybII helix (A) of a reference frame. Subsequently, the probability density of the backbone particles of the second helix (B) relative to A was calculated for periods of 100 ns after 400 ns and 4.9 μs of simulation time to assess the packing convergence of dimer association over time.

Binding orientation analysis

Preferred binding orientations in the dimer ensembles were characterized by reaction coordinates that describe the relative orientation of the dimer structures (29): the position of binding of helix B on helix A (β) and the binding phase of B (ϕ) or, alternatively, by the relative binding position χ (see Fig. 2 for a sketch on the angles). The binding position (β) is defined by the rotation angle of B relative to A in the reference structure, the binding phase (ϕ) refers to the rotation of B around its helical axis, and the relative binding position (χ) denotes the rotational angle of A relative to B.

The two parameters β and ϕ were calculated for all configurations with a COM distance between the helices below a cutoff distance. The latter is given by the first maximum in the PMF profiles (see above), defined separately for the wt and the mutants. Two-dimensional probability density distributions are presented for the two orientational parameters β and χ.

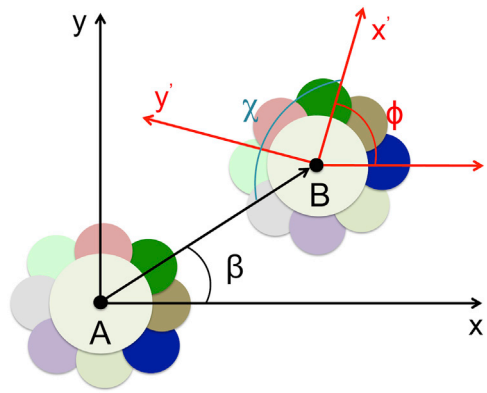

FIGURE 2 Reaction coordinates used to describe the relative orientation of two interacting sybII helices. The rotational angle of helix B relative to the reference helix A (β, binding position), the rotational angle of helix B around its own helical axis (binding phase ϕ) with respect to the reference structure, and the relative binding position (χ) defined as the rotational angle of helix A relative to helix B, are used to describe the association states of sybII TM helices. To see this figure in color, go online.

RESULTS

The dimerization of sybII TMD was studied in coarse-grained MD simulations. The influence of the specific sequence was addressed by replacing the hydrophobic stretch (residues 97–112) by valine (PolyV), isoleucine (PolyI), or leucine (PolyL). Experimentally, PolyL peptides were shown to have a low fusogenic activity, while fusion was enhanced for peptides with high valine content. Additionally, we analyzed the influence of the conserved tryptophans on TMD association.

TM helix association

The self-association of sybII TMD and a number of mutants within a POPC bilayer was studied in coarse-grained molecular dynamics simulations (CG-MD). Statistical information was gained by performing 500 simulations for each system. At the beginning of each simulation, two sybII TM helices were inserted perpendicular to the membrane plane with a separation distance of $\approx$4.5 nm to exclude intermolecular interactions. After 5 μs of simulation time, dimers were formed in almost all systems (compare also Table 1), underlining the propensity of sybII TMDs for dimer formation.

The association of TM helices to stable dimers followed a specific pattern: upon contact of the two helices, a subsequent tilting was observed, which finally led to the formation of a crossed dimer (Fig. 3). In almost all simulations (464 out of 500 runs) for wt sybII, the dimer formation was initiated by C-terminal contacts between the helices, forming a V-shaped dimer (denoted as *D2* in Fig. 3), followed by an increase of the interaction surface thereby forming a compact dimer. Two dimer conformations could be distinguished, these being a left-handed (LH) dimer and a right-handed (RH) dimer, displayed in Fig. 4.

The associated bimodal distribution for the crossing angle (Fig. 4 *A*) was observed both for the wild-type and mutant dimers. The crossing angle of $\approx -30^\circ$ obtained for the RH dimer is in good agreement with the dimer configuration predicted in a previous study using a simulated annealing protocol combined with mutagenesis data (19). The LH dimer exhibiting a smaller crossing angle of $\approx +20^\circ$ was not resolved in previous reports. Interestingly, the relative populations between the LH and RH dimers for the wild-type and the mutants differ significantly, indicating a remarkable effect of amino-acid sequence in the hydrophobic TM portion on the preferred geometry. The wild-type and the WWAA mutant mostly adopt the RH dimer conformation with the glycine at position 100 (Gly^{100}) pointing toward the interaction surface. In contrast, Gly^{100} are oppositely oriented in the LH dimer conformation, directed away from each other. Thus Gly^{100} probably adopts an important role in maintaining the geometry of the RH dimer configuration. A similar role of a central Gly residue for dimerization was reported before for integrin TM helices (24).

TABLE 1 Number of simulations, counts of monomers, C-terminal dimers, and compact dimer populations after 5 μs of CG simulation are given for each assay

System	Number of Simulations	Monomer	C-dimer	Compact Dimer	Rate Constant (%)
WT	500	2	7	491	100.0
WWAA	500	2	8	490	75.4
PolyV	500	0	0	500	190.7
PolyL	497	15	48	434	55.8

Additionally, rate constants relative to the dimerization speed of the wt sybII (set to 100%) are presented. The rate constant was determined based on a linear fit on the time interval of 0–2 μs assuming a first-order reaction. All systems show a linear behavior in this time interval.

The LH dimer is significantly more populated for PolyL, PolyI, and PolyV dimers (increasing in percentage) as compared to wt and the WWAA mutant.

In particular, the PolyV dimer showed a comparable population for LH and RH dimers. A detailed inspection of the trajectories for representative dimer structures indicates that the stability of the dimer structure correlates with its relative population. The wild-type LH dimer represents an intermediate structure, which tends to convert to a more stable RH dimer conformation that accounts for $\approx$98% of the entire final dimer ensemble. In contrast, the stability of the LH dimer for the PolyV mutant is significantly increased and the conformation is well maintained over the entire 5 μs of simulation time, resulting in a final population of $\approx$39% for the LH dimer. Unexpectedly, no LH dimer conformations were observed in the case of the WWAA mutant after 5 μs of simulation time. Additionally, the RH crossing-angle distribution is shifted by 8° to a larger crossing angle. These changes suggest a possibly important role of the membrane interfacial tryptophans not only for the membrane insertion depth (27) but for the packing of sybII helices as well.

The initial association time between helices was typically within 100–400 ns, showing no significant difference between the wild-type and mutant systems. Dissociation events leading to separation of the helices were not observed in the ensemble over the entire 5 μs of simulation time, i.e., no dissociation was seen for a total simulation time of ~10 ms.

Energetic characterization of sybII dimers

To explore the free energy of dimer association of the wild-type and mutant peptides, we calculated the PMF as a function of the COM distance between the helices analyzed from the CG simulations.

For the self-association of wild-type peptides, the PMF profiles were also calculated over different time regions to monitor the convergence, as shown in Fig. 5 (*top panel*). The shape of the PMF profiles is globally similar at different points in time. However, the PMF profiles are not converged

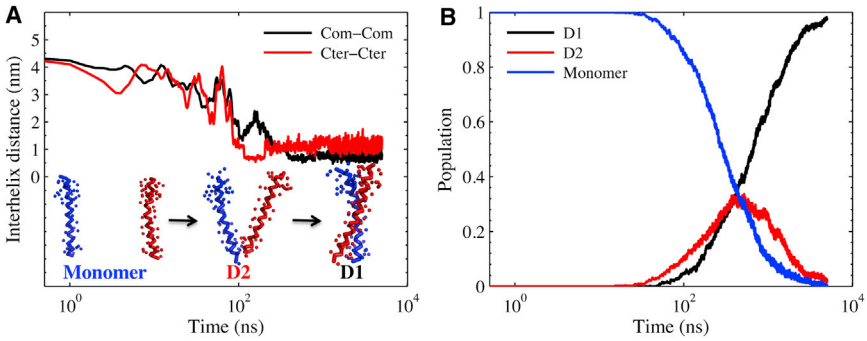

FIGURE 3 Self-association process of synaptobrevin TM helices as obtained in CG-MD simulations. (*A*) A representative dimerization process is shown for the approach of helices (COM distance of helices) as a function of simulation time (0–5 μs). (*Bottom row*) Structures representing the monomeric initial state (*left*, *Monomer*), an intermediate state (a V-shaped dimer, *D2*, *middle*), and a compact dimer (*D1*, *right*). (*B*) Population of sybII wt monomer and dimer configurations as a function of simulation time, indicating the rearrangement of initially formed intermediate D2 dimer configurations to a compact sybII dimer (D1). To see this figure in color, go online.

because no dissociation events could be observed on the simulation timescale. Strictly speaking, only PMF-like profiles are shown in Figs 5 and 6. Initially, after 500 ns, two local minima with similar energies are seen for the bound state at ~0.75 and 1.0 nm COM distance. As shown in Fig. 5 (*bottom* and *middle panels*), these minima differ in the binding phase ϕ, i.e., the dimers differ in the interaction interface. The second minimum at 1 nm vanished after 3 μs, indicating a slow convergence of PMF profiles to a single state for dimer association. The slow convergence of PMF profiles implies the necessity for long simulation times ($\approx$2–3 μs for the wild-type and mutants in this study) to obtain sufficient sampling of preferred orientations.

PMF-like profiles for both wild-type and mutants sampled at 5 μs are shown in Fig. 6 *A*. A similar PMF profile as for the wild-type was observed for the WWAA mutant, with the minimum located at $\approx$0.6 nm, suggesting a slightly closer packing for the WWAA dimer. In contrast, the dimer states of the PolyV and PolyL mutants were found at a COM distance of $\approx$1.0 nm, indicating a more loose packing of the dimers as compared to the wild-type. A possible reason for the changed packing is due to the substitution of the Gly^{100} residue in the TM core by more bulky Ile, Leu, or Val residues. Gly is known to be essential for tight helix-helix association. Interestingly, a second minimum (at $\approx$2.2 nm), which corresponds to a weakly bound dimer, quickly disappeared for the PolyV, resulting in faster kinetics for the helix-helix association for the PolyV mutant (Fig. 6 *D*). This can also be verified by the fast convergence of the average interaction energy for the whole ensemble as a function of simulation time, as shown in Fig. 6 *B*.

Dimerization kinetics

The time development of the average interaction energy for the ensemble of dimerization simulations is comparable for the wild-type and the mutants within the initial 0.5 μs (Fig. 6 *B*). On longer times, after association, kinetics is significantly decreased for the PolyL mutant and slightly increased for the PolyV mutant. The WWAA mutant displays an association kinetics similar to the wild-type.

To quantify the dimerization propensity, we calculated the quantity of compact dimers as a function of simulation time for the whole simulation ensembles (Table 1). A compact or stable dimer (see, e.g., Fig. 4 *B*) is defined by a COM distance between the helices below the distance corresponding to the first peak of the PMF profile (see the previous section).

To study the dimer structures evolution, we also calculated the population of dimer structures with only contact of the C-termini (D2). The dimerization process starts with a contact between the C-termini, followed by a subsequent conversion to a more stable dimer (D1) in most simulations (see above).

Consistent with the PMF profiles for dimer association, the quantity of stable dimers for the PolyV mutant is larger as compared to the wild-type. The rate of formed dimers (Fig. 6 *C*) is significantly reduced for the PolyL mutant

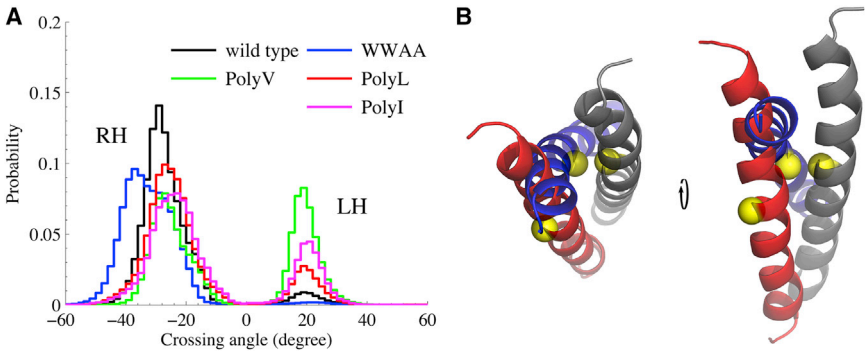

FIGURE 4 (*A*) Helix crossing-angle distribution for the sybII wild-type and mutants computed over the total simulation time (5 μs). (*B*) Representative structures from CG-MD simulations (after conversion to an all-atom representation (38)) for the right-handed (*RH*, *blue*) and left-handed (*LH*, *red*) dimer conformations (wild-type). The reference TM helix (*gray*); G100 residues (*yellow spheres*). To see this figure in color, go online.

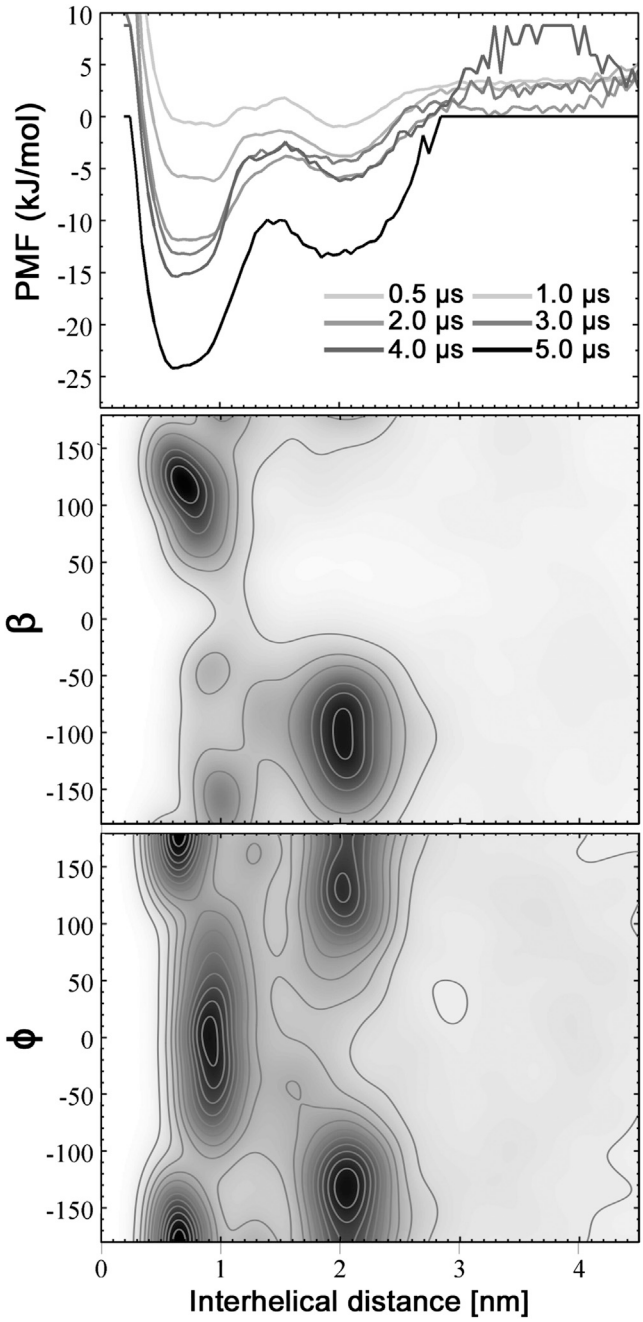

FIGURE 5 Association of wild-type helices characterized by the one-dimensional PMF as a function of the interhelical distance (COM) at different times (*top panel*, analyzed on time windows of 100 ns each). The correlations between the rotation of helix B relative to A (β, *middle panel*), and the rotation of helix B around its helical axis (ϕ, *bottom panel*) as a function of interhelical distance, are shown for $t = 500$ ns only to distinguish the distinct states in the PMF profile.

with respect to the wild-type and strongly promoted for the PolyV mutant as compared to the wild-type. Thus the dimerization kinetics may be considerably influenced by the TM sequence. In contrast, only little influence of the membrane interfacial tryptophans on the dimerization kinetics of sybII was found.

Dimer packing distribution

The lateral distribution of the second helix (B) relative to the first sybII helix (A) is shown in Fig. 7. The probability density for helix B around helix A was calculated for 100-ns windows after short (500 ns, *upper panel*) and long trajectories (5 μs, *lower panel*). Three regions (I, II, and III) of increased packing density were observed for the wild-type system at 500 ns, which correspond to distinct packing modes as displayed in Fig. 7. Right-handed (RH) dimers are found in regions I (*yellow*, I-c1 configuration, and *blue*, I-c2 configuration), II (*cyan*), and III (*red*). Left-handed (LH) dimers are restricted to region II (*green*). A comparison to the probability density map after 5 μs yields a depleted region II that includes both LH and partially RH dimers, implying metastability of configurations in this region. Region I is the most populated region in phase space after 5 μs. Region III also shows a substantial stability over the full simulation time of 5 μs. However, after extension of selected simulations to 25 μs (data not shown), all dimer configurations passed over to a specific configuration within region I (I-c1; see the following section).

The packing density for the WWAA mutant after 5 μs is similar to the wild-type. Unexpectedly, the PolyV dimer exhibited a highly promiscuous binding interface over the whole simulation time. This nonspecific association behavior may provide an explanation for the observed fast kinetics (see above). PolyL and PolyI mutants display a similar packing at 500 ns, explained by their very similar force-field parameters in the MARTINI force field (only slightly distinct bond lengths between backbone and side-chain beads). For this reason, only the PolyL mutant was extended to the full simulation time (5 μs). PolyL displays predominantly one dimer configuration with both RH and LH dimers, as described above (Fig. 4).

Two-dimensional orientational distribution

The dimer configurations were characterized further using the binding position β, describing the position of the second helix with respect to the reference helix, and the relative binding position χ analyzed over the final 50 ns of the 5-μs simulations (Fig. 8). The most populated dimer configuration (I-c1) is similar for both wt and mutant systems (compare Table 2). In addition, alternative binding interfaces (I-c2 and III, or *E*) with significant populations were observed. SybII and the WWAA mutant showed the same alternative binding modes with similar populations.

In agreement with the packing density, the PolyV dimer does not show a strong preference for a single specific binding interface. It adopts an additional configuration (termed *E*) as compared to the wt with a high probability (>40%). This is in agreement with a previous experimental

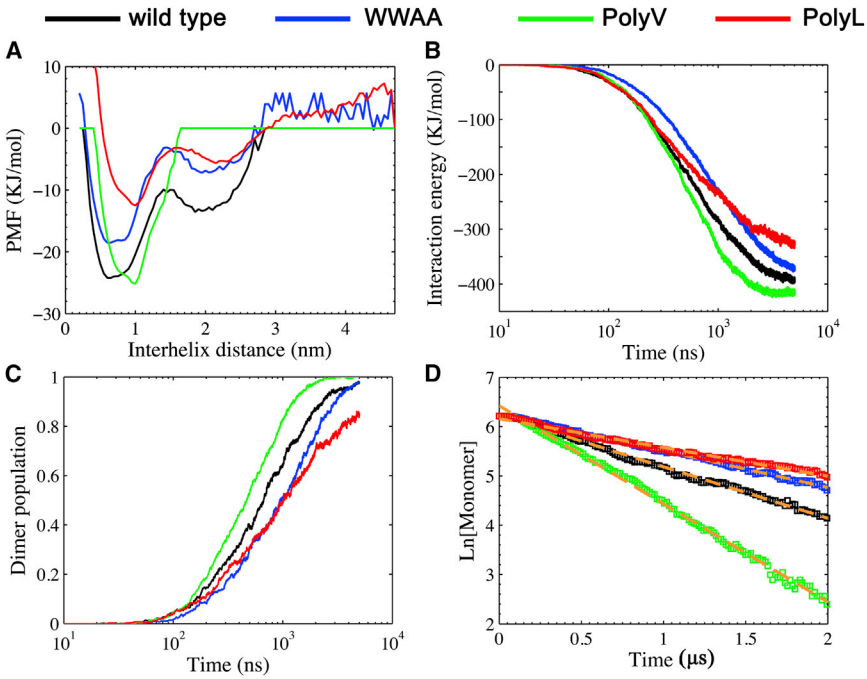

FIGURE 6 Comparison of dimerization kinetics for wild-type and mutants. (*A*) One-dimensional PMF as a function of interhelical distance at 5 μs. (*B*) Convergence of mean interaction energy between helices. (*C*) Population of compact dimers over the entire ensembles (500 runs) as a function of simulation time. (*D*) Logarithm of the concentration of monomers as a function of simulation time and fit (*dashed lines*) assuming a first-order reaction. The reaction constant is given by the slope of the linear fit (between 0 and 2 μs) and shown in Table 1. To see this figure in color, go online.

study on a Val-based TM peptide (V16) flanked by lysines and tryptophan that led to massive lipid-peptide aggregates (50). Thus, the number of available binding interfaces and the packing probability do appear to be correlated with the degree of TM helix aggregation.

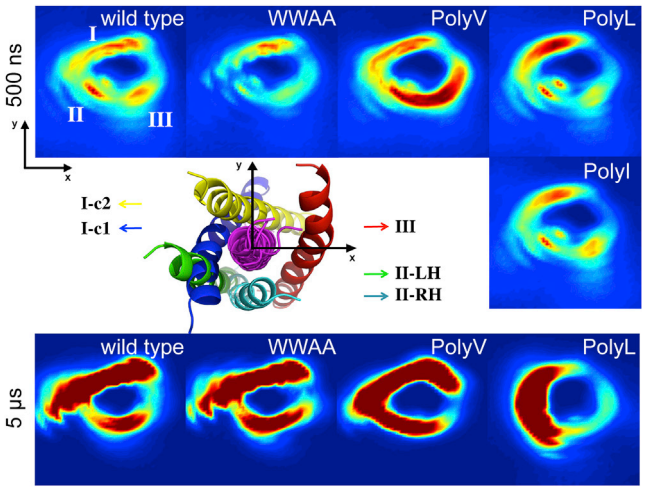

FIGURE 7 Packing-density distribution of sybII helix B relative to the reference helix A of the wild-type and mutants by CG-MD simulation at 500 ns (*top panel*) and 5 μs (*bottom panel*) as a function of lateral position (*x*-*y*). Representative CG-dimer structures of the wild-type were converted to atomistic resolution with the reference helix A indicated (*magenta*). I-c1 (*blue*) and I-c2 (*yellow*) dimers correspond to region I; LH (*green*) and RH (*cyan*) dimers to region II; (*red*) region III. (A gradient color scheme from *blue* to *red* represents low to high density of states.) The PolyI mutant simulation was not extended to the full simulation time (5 μs) due to its similarity to PolyL in the coarse-grained force field. To see this figure in color, go online.

Structural validation by atomistic MD simulations

Selected coarse-grained dimer configurations were further inspected and validated by subsequent atomistic MD simulations; CG model structures were first converted to atomistic representations using the BACKWARD algorithm (38), followed by atomistic (AA) MD simulation using both the CHARMM36 force field and the AMBER/SLIPIDS force fields for comparison. The conformational stability was addressed for three sybII wt dimer configurations (I-c1, I-c2, and III) as well as for the most populated dimer configurations for WWAA, PolyV, PolyI, and PolyL (I-c1) by comparing the backbone root-mean-square deviation (RMSD) obtained in 200-ns MD simulations (Fig. 9). Overall, the dimer configurations were stable, with RMSD values between 2 and 4 Å; the exception was the PolyI mutant, which displayed the largest flexibility with RMSD values ranging up to 6 Å for both force fields.

Those residues contributing favorably to dimer formation were pinpointed by analyzing their contribution to the total interaction energy between the helices (restricted to van der Waals and Coulomb interactions averaged over the final 50 ns of the simulations). The analysis was restricted to the most populated conformation of the sybII wt TM helix (I-c1). As shown in Fig. 10, Leu^{99}, Cys^{103}, Leu^{107}, and Ile^{111} contribute most strongly to helix-helix association within the hydrophobic part of the TM helix (residues 97–112), in good agreement with previous mutagenesis and computational studies (17,19). These four residues are located on the same side of the TM helix, forming, together with M95 and M96, the symmetric binding interface of the sybII dimer (see Fig. 11, *left panel*). The other two residues

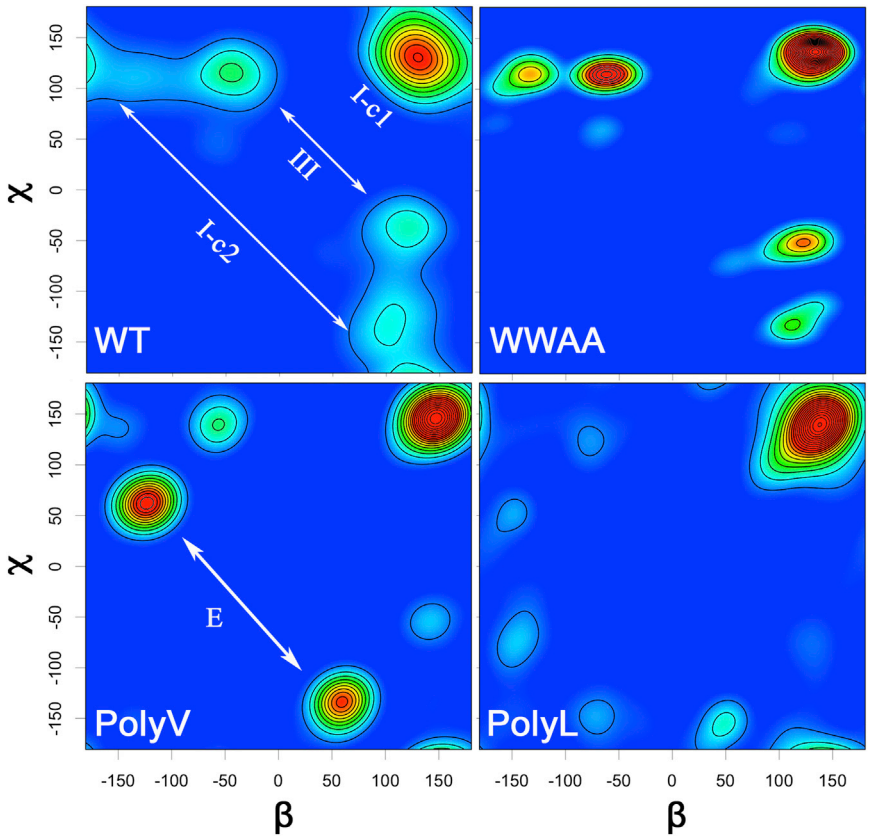

FIGURE 8 Two-dimensional orientational analysis of dimer ensemble by the probability distribution of binding position (β) and relative binding position (χ) for wild-type and mutant sequences. The regions corresponding to dimer configurations representative of dimer I-c1, I-c2, and III are highlighted in the wild-type sybII TM helix plot. An extra configuration (E) is pointed to in the PolyV plot. To see this figure in color, go online.

important for sybII dimerization as predicted by experiment, I102 and I110, were found to contribute to the asymmetric binding interfaces I-c2 and III, respectively (Fig. 11, *middle* and *right panels*). Consistent results were obtained for both AMBER and CHARMM36 force fields.

DISCUSSION

The TMD of SNARE proteins was previously shown to be essential for its fusion activity (8,23,51). For synaptobrevin II, the TMD was shown to form dimers and higher-order oligomers (17). This interaction between the TMDs is thought to be critical for the transition from hemifusion to complete fusion (22). Here we applied multiscale simulations to investigate the TMD homodimerization of sybII and a range of mutants and characterized the influence of mutations on dimerization. In order to fully sample the accessible conformational space for dimerization, i.e., to sample alternative binding modes for the TM peptides, 500 simulations were performed for each system. Metastable states exhibited a stability on the timescale of nanoseconds to microseconds. Accordingly, the simulation length was chosen to be 5 μs. This timescale allows us to distinguish subtle differences in the relative populations of distinct dimer configurations and enables the identification of the main binding modes as well as the relative stabilities of different conformations. Still, the distribution of states is not likely to be fully equilibrated on this timescale.

TABLE 2 Populations of different dimerization interfaces at 5 μs as determined from orientation analysis

System	I-c1	III	I-c2	*E*
WT	48.6	26.2	21.2	—
WWAA	48.5	27.7	17.1	—
PolyV	41.1	11.0	2.7	40.6
PolyL	73.9	6.6	—	8.1

In this study, the wild-type sybII and all the mutants formed stable dimers. A previous experimental study has shown that an oligo-leucine (L16) peptide could form dimers in both solution and membrane environments (52). Dimerization was comparably low for a differently bordered poly-leucine peptide (R at N-terminus, RRLI at C-terminus) (53). Langosch et al. (14) showed further that L16 with flanking Lys residues is ineffective in promoting the liposome-liposome fusion upon incorporation into membranes, while the peptide harboring the TMD core of sybII significantly enhances fusion kinetics. In addition, TM peptides containing a mixture of Val and Leu residues have been shown to be active in promoting membrane fusion, and the fusion activity was reported to be increased for high Val contents (50). In line with these experimental studies, the PolyL mutant displayed in the CG simulations a considerably decreased dimerization kinetics and less compact dimers (see below), while it was increased for the PolyV

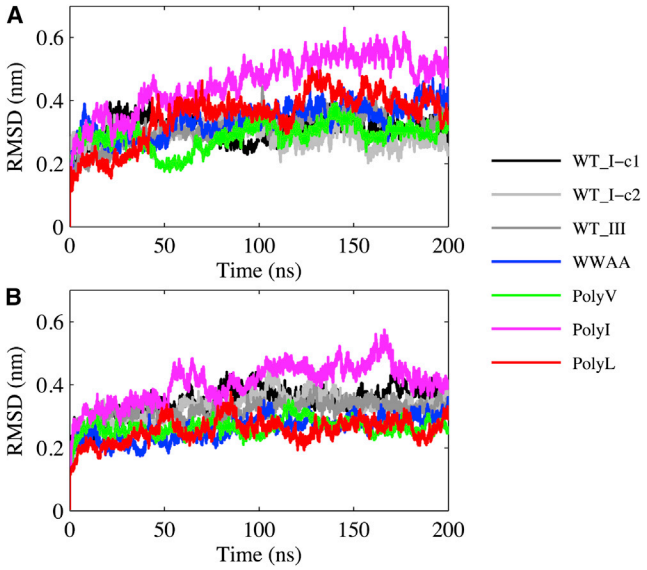

FIGURE 9 Conformational stability of representative sybII TM helix dimer configurations measured by the backbone RMSD from the starting configuration for both the AMBER (*A*) and CHARMM36 (*B*) force fields. To see this figure in color, go online.

mutant. The highly promiscuous binding interface of the PolyV mutant enables fast binding. This also agrees with earlier experimental results, which showed that poly-valine peptides could overaggregate in micelles (14,50), corroborating our simulation results.

In the majority of the dimerization events, the formation of a stable dimer was preceded by C-terminal contacts. This suggests that the C-terminus plays a possible role in promoting the association. The C-terminal part of sybII has previously been shown to be involved in the formation of the fusion pore (10,54). Additionally, a previous FRET study reported C-terminal interactions upon association of SNARE proteins (12). The content mixing involved in the final stage of membrane fusion was reported to be abolished when the C-terminal half of the TMD is deleted (8), suggesting an essential role of the C-terminal part in the final stage of membrane fusion. However, it remains to be shown how the fusion activity is influenced by the C-terminus.

The sybII homodimer interface predicted from our simulations is consistent with previous mutagenesis and computational studies (17,19). The four residues (L99, C103, L107, and I111) in the dominant dimer configuration (I-c1, see Fig. 11) constitute a well-defined binding interface in the hydrophobic core (residues 97–112) of sybII TMD (Fig. 10). The largest effect of a single-point mutation on binding is expected for such mutations at the I-c1 dimer interface in particular, due to both its symmetry and restricted number of side chains interacting with the partner. The asymmetric I-c2 dimer possesses a comparably extended dimerization interface with many residues contributing (in detail: residues I97, L99, V101, A104, I105, L107, and I108 of one monomer interact with I98, I102, I105, I106, and I110 of the other monomer). However, most of those residues point sideways from the dimerization interface, and thus the exchange of one of them for an alanine mutant will probably only moderately reduce the dimerization propensity.

Besides the above-identified residues within the hydrophobic core of sybII TMD that contribute to helix-helix interaction, two adjacent residues M95/M96 also showed substantial contributions (see Fig. 10), suggesting a role of these two residues for sybII TMD homodimerization. A previous experimental study on the sybII TMD construct reported a remarkable promotion of self-association upon substitution of Leu by Met residues, possibly by facilitating the formation of a disulfide bond between the helices (18). It is also interesting to note that W89/W90 are directed away from the binding interface for the most populated dimer configuration (I-c1) and thus hardly contribute to dimer stability. Accordingly, the WWAA mutant displays only small differences in dimer packing and dimerization kinetics as compared to the wild-type.

Despite the similarity of the dimerization behavior between the wild-type and the WWAA mutant, subtle

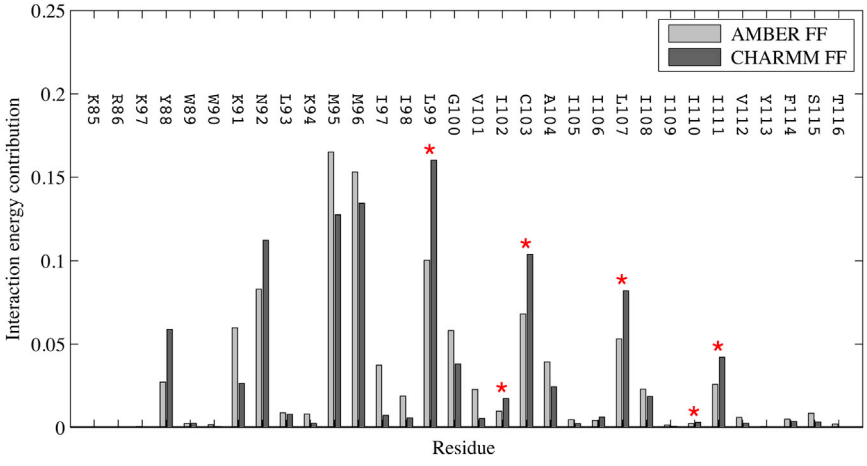

FIGURE 10 Interaction energy contribution for individual residues to the helix-helix association for the most populated dimer (I-c1) in wild-type sybII simulation. (*Red stars*) Residues critical to the dimerization obtained in experiments (17,19). Interaction energies were approximated as the sum of (short-range) Lennard-Jones and electrostatic contributions. To see this figure in color, go online.

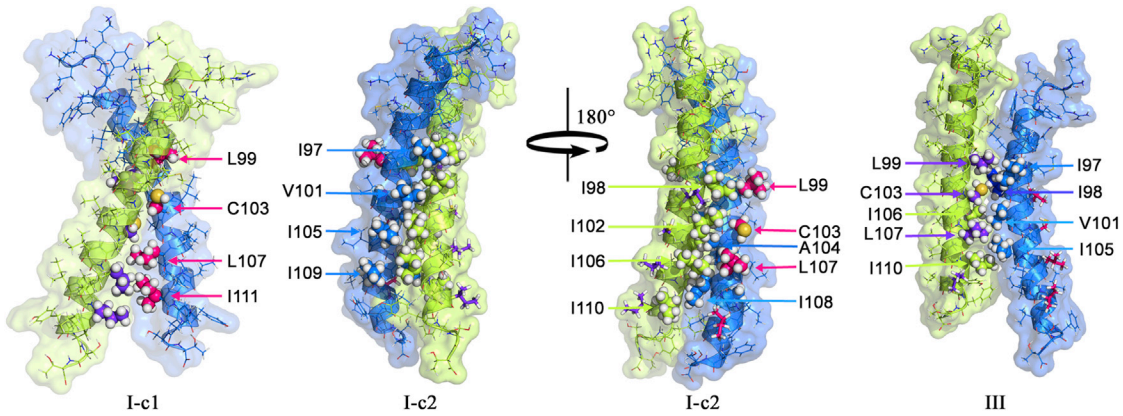

FIGURE 11 Comparison of binding interfaces for representative dimer structures of the wild-type sybII TMD in AA-MD simulations. For the dimer I-c1, a symmetric packing interface is seen, consisting of L99, C103, L107, and I111 in the hydrophobic part of the TM (highlighted by *magenta* and *purple spheres*). The asymmetric I-c2 dimer possesses a comparably extended dimerization interface displayed from two perspectives. The average helix crossing-angle for I-c1 is ≈50°, for I-c2 is 30°, and for dimer configuration III, 19° (calculated for CHARMM36). To see this figure in color, go online.

differences were identified for the helix packing. The packing of the WWAA dimer is more compact (see Fig. 8), reflecting a comparably more flexible binding interface for the wild-type. The interfacial tryptophan residues thus may adopt a role in maintaining the flexibility of sybII dimers, thereby possibly facilitating the interconversion between the SNARE proteins (i.e., from homodimer to heterodimer), which is considered to be essential in the final stage of membrane fusion (2,5). It is also interesting to note that PolyV forms the alternative binding interface *E* instead of I-c2 (wt) (Fig. 8). This is explained by the replacement of G100 in the hydrophobic core of sybII TMD, known to play an important role in helix-helix packing (24,55). E.g., the packing of the GpA dimer was reported to be disrupted upon the mutations of key glycine residues, with the geometry preference lost and flexibility increased (55). For integrin heterodimers consisting of αIIb and β3 TM helices, weaker helix packing interactions were found for mutated glycine residues in the central TM domain of αIIb (24). In the PolyV mutant, the Gly substitution also results in a larger helix separation distance as compared to the wt, reflected by the one-dimensional PMF.

Although two alternative binding interfaces are observed for the wild-type or WWAA mutant, the synaptobrevin homodimer flexibility appears to be functionally important for effective SNARE-mediated membrane fusion. In other words, at the priming stage of membrane fusion, the stable synaptobrevin homooligomer may help to establish an efficient contact between two opposing membranes before the formation of the hemifusion state. A further evolution of the hemifusion state requires the continuous zipping of SNARE proteins extending to the TMD core (forming synaptobrevin/syntaxin TMD heterooligomers), which would pull the distal leaflet closer to form a fusion pore. Thus, a synaptobrevin TMD homooligomerization of optimal strength is important during this process, which makes the synaptobrevin oligomer more accessible for the interaction with its syntaxin partner.

The formation of sybII oligomers consisting of two to four monomers was reported in a previous study, albeit the concentration of higher-order oligomers was relatively small as compared to dimers. The formation of higher-order oligomers was probably suppressed due to sterical hindrance of the fused soluble nuclease-A protein (17). Alternative sybII binding interfaces to the one reported previously are essential to explain the higher-order oligomerization. The above-described different dimerization interfaces indeed allow for the formation of higher-order oligomers, as shown in Fig. 12 for a trimer and a tetramer modeled from the different dimer configurations.

In addition, the cooperativity of several SNARE complexes is required for efficient membrane fusion, with the number of complexes reported to range between two and eight (12,56–62). This supracomplex was proposed to be mediated by the TMD of SNARE proteins (13). A recent

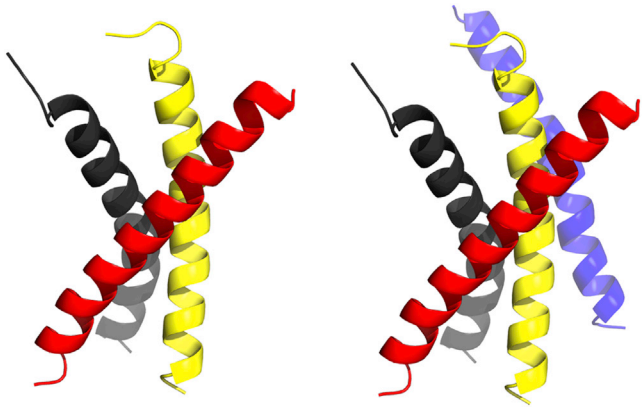

FIGURE 12 Models for sybII homotrimer and -tetramer structures based on the binding interfaces displayed in Fig. 11. To see this figure in color, go online.

study suggested a model in which the number of SNAREs required for fusion is greatly variable and dependent on the biological conditions (63). However, the functional organization and dynamics of SNARE proteins and complexes is only partially understood.

The alternative binding modes observed in the wild-type, but not in the PolyL mutant, explain the experimental finding that a poly-leucine mutant has a low fusogenic activity (14,50). The alternative binding interfaces of sybII dimerization adopt an important functional role for higher-order oligomerization required for fusion.

In conclusion, the dimerization of the sybII TM helix and selected mutants was characterized by multiscale simulation on the basis of a high-throughput approach. The wild-type sequence of sybII appears to be optimized for fast binding as well as for display of different interaction surfaces. The latter is suggested to be required for further oligomerization possibly required for membrane fusion.

AUTHOR CONTRIBUTIONS

R.A.B. designed research; J.H. performed simulations; J.H., K.P., and T.A.W. did the analysis; and J.H., K.P., T.A.W., and R.A.B. wrote the article.

ACKNOWLEDGMENTS

Computer time was provided by the Computing Center of the University Erlangen-Nürnberg.

This work was supported by the Deutsche Forschungsgemeinschaft under project No. BO2963/2-1 and Research Training Group grant No. 1962, "Dynamic Interactions at Biological Membranes—From Single Molecules to Tissue" (to J.H., K.P., and R.A.B.). This work was also supported by a scholarship from the China Scholarship Council (to J.H.) and by the emerging field initiative "Synthetic Biology" of the Friedrich-Alexander University of Erlangen-Nürnberg (to T.A.W. and R.A.B.).

REFERENCES

1. Li, L., and L.-S. Chin. 2003. The molecular machinery of synaptic vesicle exocytosis. *Cell. Mol. Life Sci.* 60:942–960.
2. Südhof, T. C. 2013. Neurotransmitter release: the last millisecond in the life of a synaptic vesicle. *Neuron.* 80:675–690.
3. Jahn, R., and D. Fasshauer. 2012. Molecular machines governing exocytosis of synaptic vesicles. *Nature.* 490:201–207.
4. Sutton, R. B., D. Fasshauer, …, A. T. Brunger. 1998. Crystal structure of a SNARE complex involved in synaptic exocytosis at 2.4 Å resolution. *Nature.* 395:347–353.
5. Stein, A., G. Weber, …, R. Jahn. 2009. Helical extension of the neuronal SNARE complex into the membrane. *Nature.* 460:525–528.
6. Min, D., K. Kim, …, T.-Y. Yoon. 2013. Mechanical unzipping and rezipping of a single SNARE complex reveals hysteresis as a force-generating mechanism. *Nat. Commun.* 4:1705.
7. Gao, Y., S. Zorman, …, Y. Zhang. 2012. Single reconstituted neuronal SNARE complexes zipper in three distinct stages. *Science.* 337:1340–1343.
8. Xu, Y., F. Zhang, …, Y.-K. Shin. 2005. Hemifusion in SNARE-mediated membrane fusion. *Nat. Struct. Mol. Biol.* 12:417–422.
9. Xu, H., M. Zick, …, Y. Jun. 2011. A lipid-anchored SNARE supports membrane fusion. *Proc. Natl. Acad. Sci. USA.* 108:17325–17330.
10. Ngatchou, A. N., K. Kisler, …, M. Lindau. 2010. Role of the synaptobrevin C terminus in fusion pore formation. *Proc. Natl. Acad. Sci. USA.* 107:18463–18468.
11. Fdez, E., M. Martínez-Salvador, …, S. Hilfiker. 2010. Transmembrane-domain determinants for SNARE-mediated membrane fusion. *J. Cell Sci.* 123:2473–2480.
12. Lu, X., Y. Zhang, and Y.-K. Shin. 2008. Supramolecular SNARE assembly precedes hemifusion in SNARE-mediated membrane fusion. *Nat. Struct. Mol. Biol.* 15:700–706.
13. Mascia, L., and D. Langosch. 2007. Evidence that late-endosomal SNARE multimerization complex is promoted by transmembrane segments. *Biochim. Biophys. Acta.* 1768:457–466.
14. Langosch, D., J. M. Crane, …, J. Reed. 2001. Peptide mimics of SNARE transmembrane segments drive membrane fusion depending on their conformational plasticity. *J. Mol. Biol.* 311:709–721.
15. Laage, R., J. Rohde, …, D. Langosch. 2000. A conserved membrane-spanning amino acid motif drives homomeric and supports heteromeric assembly of presynaptic SNARE proteins. *J. Biol. Chem.* 275:17481–17487.
16. Margittai, M., H. Otto, and R. Jahn. 1999. A stable interaction between syntaxin 1a and synaptobrevin 2 mediated by their transmembrane domains. *FEBS Lett.* 446:40–44.
17. Laage, R., and D. Langosch. 1997. Dimerization of the synaptic vesicle protein synaptobrevin (vesicle-associated membrane protein) II depends on specific residues within the transmembrane segment. *Eur. J. Biochem.* 249:540–546.
18. Kroch, A. E., and K. G. Fleming. 2006. Alternate interfaces may mediate homomeric and heteromeric assembly in the transmembrane domains of SNARE proteins. *J. Mol. Biol.* 357:184–194.
19. Fleming, K. G., and D. M. Engelman. 2001. Computation and mutagenesis suggest a right-handed structure for the synaptobrevin transmembrane dimer. *Proteins.* 45:313–317.
20. Bowen, M. E., D. M. Engelman, and A. T. Brunger. 2002. Mutational analysis of synaptobrevin transmembrane domain oligomerization. *Biochemistry.* 41:15861–15866.
21. Roy, R., R. Laage, and D. Langosch. 2004. Synaptobrevin transmembrane domain dimerization—revisited. *Biochemistry.* 43:4964–4970.
22. Hofmann, M. W., K. Peplowska, …, D. Langosch. 2006. Self-interaction of a SNARE transmembrane domain promotes the hemifusion-to-fusion transition. *J. Mol. Biol.* 364:1048–1060.
23. Langosch, D., M. Hofmann, and C. Ungermann. 2007. The role of transmembrane domains in membrane fusion. *Cell. Mol. Life Sci.* 64:850–864.
24. Kalli, A. C., B. A. Hall, …, M. S. Sansom. 2011. A helix heterodimer in a lipid bilayer: prediction of the structure of an integrin transmembrane domain via multiscale simulations. *Structure.* 19:1477–1484.
25. Reddy, T., S. Manrique, …, M. S. Sansom. 2014. Primary and secondary dimer interfaces of the fibroblast growth factor receptor 3 transmembrane domain: characterization via multiscale molecular dynamics simulations. *Biochemistry.* 53:323–332.
26. Sengupta, D., and S. J. Marrink. 2010. Lipid-mediated interactions tune the association of glycophorin A helix and its disruptive mutants in membranes. *Phys. Chem. Chem. Phys.* 12:12987–12996.
27. Borisovska, M., Y. N. Schwarz, …, D. Bruns. 2012. Membrane-proximal tryptophans of synaptobrevin II stabilize priming of secretory vesicles. *J. Neurosci.* 32:15983–15997.
28. Monticelli, L., S. K. Kandasamy, …, S.-J. Marrink. 2008. The MARTINI coarse-grained force field: extension to proteins. *J. Chem. Theory Comput.* 4:819–834.
29. Wassenaar, T. A., K. Pluhackova, …, R. A. Böckmann. 2015. High-throughput simulations of dimer and trimer assembly of membrane proteins. The DAFT approach. *J. Chem. Theory Comput.* 11:2278–2291.

30. Pluhackova, K., T. A. Wassenaar, …, R. A. Böckmann. 2015. Spontaneous adsorption of coiled-coil model peptides K and E to a mixed lipid bilayer. *J. Phys. Chem. B.* 119:4396–4408.

31. Hess, B., C. Kutzner, …, E. Lindahl. 2008. GROMACS 4: algorithms for highly efficient, load-balanced, and scalable molecular simulation. *J. Chem. Theory Comput.* 4:435–447.

32. Schrödinger LLC. 2010. The PYMOL Molecular Graphics System, Ver. 1.3r1. http://www.schrodinger.com/.

33. Pluhackova, K., T. A. Wassenaar, and R. A. Böckmann. 2013. Molecular dynamics simulations of membrane proteins. *In* Membrane Biogenesis, Vol. 1033, Methods in Molecular Biology. D. Rapaport and J. M. Herrmann, editors. Humana Press, Totowa, NJ, pp. 85–101.

34. Wassenaar, T. A., H. I. Ingólfsson, …, S.-J. Marrink. 2015. Computational lipidomics with insane: a versatile tool for generating custom membranes for molecular simulations. *J. Chem. Theory Comput.* 11:2144–2155.

35. Wassenaar, T. A., H. I. Ingólfsson, …, L. V. Schäfer. 2013. Mixing MARTINI: electrostatic coupling in hybrid atomistic-coarse-grained biomolecular simulations. *J. Phys. Chem. B.* 117:3516–3530.

36. Bussi, G., D. Donadio, and M. Parrinello. 2007. Canonical sampling through velocity rescaling. *J. Chem. Phys.* 126:014101.

37. Berendsen, H. J. C., J. P. M. Postma, …, J. R. Haak. 1984. Molecular dynamics with coupling to an external bath. *J. Chem. Phys.* 81:3684–3690.

38. Wassenaar, T. A., K. Pluhackova, …, D. P. Tieleman. 2014. Going BACKWARD: a flexible geometric approach to reverse transformation from coarse grained to atomistic models. *J. Chem. Theory Comput.* 10:676–690.

39. Best, R. B., X. Zhu, …, A. D. Mackerell, Jr. 2012. Optimization of the additive CHARMM all-atom protein force field targeting improved sampling of the backbone φ, ψ, and side-chain $\chi(1)$ and $\chi(2)$ dihedral angles. *J. Chem. Theory Comput.* 8:3257–3273.

40. Lindorff-Larsen, K., S. Piana, …, D. E. Shaw. 2010. Improved side-chain torsion potentials for the AMBER ff99SB protein force field. *Proteins.* 78:1950–1958.

41. Jämbeck, J. P. M., and A. P. Lyubartsev. 2012. Derivation and systematic validation of a refined all-atom force field for phosphatidylcholine lipids. *J. Phys. Chem. B.* 116:3164–3179.

42. Jämbeck, J. P. M., and A. P. Lyubartsev. 2012. An extension and further validation of an all-atomistic force field for biological membranes. *J. Chem. Theory Comput.* 8:2938–2948.

43. Parrinello, M., and A. Rahman. 1981. Polymorphic transitions in single crystals: a new molecular dynamics method. *J. Appl. Phys.* 52:7182–7190.

44. Nosé, S. 1984. A molecular dynamics method for simulations in the canonical ensemble. *Mol. Phys.* 100:191–198.

45. Hoover, W. G. 1985. Canonical dynamics: equilibrium phase-space distributions. *Phys. Rev. A.* 31:1695–1697.

46. Hess, B., H. Bekker, …, J. G. E. M. Fraaije. 1997. LINCS: a linear constraint solver for molecular simulations. *J. Comput. Chem.* 18: 1463–1472.

47. Darden, T., D. York, and L. Pedersen. 1993. Particle mesh Ewald: an N log(N) method for Ewald sums in large systems. *J. Chem. Phys.* 98:10089–10092.

48. Torrie, G. M., and J. P. Valleau. 1977. Nonphysical sampling distributions in Monte Carlo free-energy estimation—umbrella sampling. *J. Comput. Phys.* 23:187–199.

49. Pawar, A. B., S. A. Deshpande, …, D. Sengupta. 2015. Thermodynamic and kinetic characterization of transmembrane helix association. *Phys. Chem. Chem. Phys.* 17:1390–1398.

50. Hofmann, M. W., K. Weise, …, D. Langosch. 2004. De novo design of conformationally flexible transmembrane peptides driving membrane fusion. *Proc. Natl. Acad. Sci. USA.* 101:14776–14781.

51. Rohde, J., L. Dietrich, …, C. Ungermann. 2003. The transmembrane domain of Vam3 affects the composition of *cis*- and *trans*-SNARE complexes to promote homotypic vacuole fusion. *J. Biol. Chem.* 278: 1656–1662.

52. Gurezka, R., R. Laage, …, D. Langosch. 1999. A heptad motif of leucine residues found in membrane proteins can drive self-assembly of artificial transmembrane segments. *J. Biol. Chem.* 274:9265–9270.

53. Zhou, F. X., H. J. Merianos, …, D. M. Engelman. 2001. Polar residues drive association of polyleucine transmembrane helices. *Proc. Natl. Acad. Sci. USA.* 98:2250–2255.

54. Lindau, M., B. A. Hall, …, M. S. Sansom. 2012. Coarse-grain simulations reveal movement of the synaptobrevin C-terminus in response to picoNewton forces. *Biophys. J.* 103:959–969.

55. Psachoulia, E., D. P. Marshall, and M. S. Sansom. 2010. Molecular dynamics simulations of the dimerization of transmembrane α-helices. *Acc. Chem. Res.* 43:388–396.

56. Sinha, R., S. Ahmed, …, J. Klingauf. 2011. Two synaptobrevin molecules are sufficient for vesicle fusion in central nervous system synapses. *Proc. Natl. Acad. Sci. USA.* 108:14318–14323.

57. Domanska, M. K., V. Kiessling, …, L. K. Tamm. 2009. Single vesicle millisecond fusion kinetics reveals number of SNARE complexes optimal for fast SNARE-mediated membrane fusion. *J. Biol. Chem.* 284:32158–32166.

58. Hua, Y., and R. H. Scheller. 2001. Three SNARE complexes cooperate to mediate membrane fusion. *Proc. Natl. Acad. Sci. USA.* 98:8065–8070.

59. Megighian, A., M. Zordan, …, C. Montecucco. 2013. Evidence for a radial SNARE super-complex mediating neurotransmitter release at the *Drosophila* neuromuscular junction. *J. Cell Sci.* 126:3134–3140.

60. Mohrmann, R., H. de Wit, …, J. B. Sørensen. 2010. Fast vesicle fusion in living cells requires at least three SNARE complexes. *Science.* 330:502–505.

61. Mohrmann, R., and J. B. Sørensen. 2012. SNARE requirements en route to exocytosis: from many to few. *J. Mol. Neurosci.* 48:387–394.

62. Shi, L., Q.-T. Shen, …, F. Pincet. 2012. SNARE proteins: one to fuse and three to keep the nascent fusion pore open. *Science.* 335:1355–1359.

63. Hernandez, J. M., A. J. Kreutzberger, …, R. Jahn. 2014. Variable cooperativity in SNARE-mediated membrane fusion. *Proc. Natl. Acad. Sci. USA.* 111:12037–12042.